Title: Functional connectivity across the human subcortical auditory system using a Gaussian copula graphical model approach with partial correlations

Authors: Kevin R. Sitek[1]*, Noirrit Kiran Chandra[2]*, Abhra Sarkar[3], Bharath Chandrasekaran[1]

*=contributed equally

Affiliations: (1) University of Pittsburgh, Dept. of Communication Science and Disorders; (2) The University of Texas at Dallas, Dept. of Mathematical Sciences; (3) The University of Texas at Austin, Dept. of Statistics and Data Sciences

Corresponding author:

Kevin R. Sitek (kevin.sitek@pitt.edu)

Abstract/Summary

The central auditory system is comprised of multiple subcortical brain structures that sequentially process and refine incoming acoustic signals along the primary auditory pathway. Due to the technical limitations of imaging small structures deep inside the brain, most of our knowledge of the subcortical auditory system is based on research in animal models using invasive methodologies. While recent advances in ultra-high field functional magnetic resonance imaging (fMRI) acquisition have enabled novel investigations of the human subcortex non-invasively, optimal approaches to assessing functional activation and connectivity are still being developed. Traditionally, functional connectivity using fMRI data is estimated with simple correlation matrices. Partial correlations however reveal the connectivity between two regions after removing the effects of all other regions and hence are often more meaningful. Partial correlation analysis is particularly promising in the subcortical auditory system, where sensory information is passed serially from nucleus to nucleus up the primary

auditory pathway, providing redundant but also increasingly abstract representations of auditory stimuli (Chechik and Nelken, 2012). In this project, we developed and implemented a Gaussian copula graphical model (GCGM) approach to estimate the partial correlations and thereby infer the functional connectivity patterns within the auditory system. Given the paucity of non-invasive methods for human subcortical investigations, we aim to unveil novel information about the hierarchy and direct connections throughout the human subcortical auditory system. Our results show strong positive partial correlations between contralateral structures throughout the auditory system, particularly in the auditory midbrain and thalamus. We also found positive partial correlations between successive structures in the auditory pathway on each side (left and right), including between auditory midbrain and thalamus, and between primary and associative auditory cortex. Further, we confirmed that these connectivity estimates were unique to the auditory system, as non-auditory regions included as controls—namely, visual cortex and superior frontal cortex—were strongly connected to their contralateral homologues but only minimally connected with auditory brain regions. Additionally, these results were highly stable when splitting the data in half according to the acquisition schemes and computing partial correlations separately for each half of the data, as well as across cross-validation folds. Overall, these results demonstrate that unique functional connectivity patterns along the auditory pathway are recoverable using novel connectivity approaches and that our connectivity methods are reliable across multiple acquisitions.

Keywords (6): resting state connectivity, functional MRI, partial correlation, subcortical auditory system, Gaussian copula graphical model

Funding: This work was supported by the National Science Foundation (to AS and BC) and the National Institutes of Health/National Institute on Deafness and Other Communication Disorders (K01DC019421 to KRS and R01DC01550 to BC).

1. Introduction

The mammalian auditory pathway conveys acoustic information between the inner ear—where sounds are mechanoelectrically transduced in the cochlea—and auditory cortex by way of multiple subcortical nuclei in the brainstem, midbrain, and thalamus. Much of our knowledge of the auditory system arises from anatomical and physiological research with non-human animal models. This work has contributed tremendously to our understanding of the mammalian auditory system. However, due to methodological and ethical limitations, our ability to directly assess auditory function in the human nervous system is severely constrained.

This is particularly true when it comes to subcortical auditory structures. Due to their small size—tightly packed in with other heterogeneous nuclei and white matter pathways—and their anatomical location deep within the cranium, the subcortical auditory structures have received limited attention in non-invasive human research.

Magnetic resonance imaging (MRI) methods such as functional MRI (fMRI) are one such group of non-invasive methods that have only scarcely been used to investigate the subcortical auditory system. Previous task fMRI research has functionally localized the subcortical auditory structures (Sitek *et al.*, 2019), identified the tonotopic frequency mappings in auditory midbrain and thalamus (De Martino *et al.*, 2013; Moerel *et al.*, 2015; Ress and Chandrasekaran, 2013), separated top-down and bottom-up speech-selective subregions of auditory thalamus (Mihai *et al.*, 2019; Tabas *et al.*, 2021), and recorded level-dependent BOLD signals throughout the auditory pathway (Hawley *et al.*, 2005; Sigalovsky and Melcher, 2006).

In contrast to task-related BOLD activity, fMRI connectivity methods (often utilizing resting state or passive movie watching fMRI paradigms) are commonly used to assay cortical brain networks (Biswal *et al.*, 1995; Gordon *et al.*, 2017; Power *et al.*, 2011; Smith, Beckmann, *et al.*, 2013), including the cortical auditory system (Abrams *et al.*, 2020; Cha *et al.*, 2016; Chen *et al.*, 2020; Eckert *et al.*, 2008; Maudoux *et al.*, 2012; Ren *et al.*, 2021). However, fMRI connectivity methods have limited history in human brainstem research, especially in the auditory system, where they have—to our knowledge—only been utilized a handful of times to assess

connectivity differences between individuals with and without tinnitus percepts (Berlot *et al.*, 2020; Hofmeier *et al.*, 2018; Leaver *et al.*, 2016; Zhang *et al.*, 2015).

Given the anatomical and methodological constraints with subcortical fMRI, such limited fMRI connectivity literature isn't too surprising. First, the deep location of the subcortical structures places them far from MRI transmit and receive coils, limiting the signal-to-noise ratio from these regions (Miletić *et al.*, 2020). Additionally, because the brainstem is relatively centrally located relative to the multiple receiver coils, accelerated acquisition techniques that are based on phase differences between receiver coils are less effective (Preibisch *et al.*, 2015). Second, subcortical nuclei can be quite small, requiring higher resolution imaging protocols (which unfortunately trade off SNR in order to achieve greater spatial resolution). Third, subcortical nuclei are arranged heterogeneously, so voxels immediately next to those containing core auditory structures could contain visual, motor, or sensory nuclei, white matter, CSF, or a combination of any of these. Ultimately, each of these constraints limits the SNR from subcortical auditory nuclei.

Recent advances in MRI acquisition have facilitated subcortical auditory investigations. Perhaps the largest advance is the wider adoption of 7 Tesla (7T) MRI for human cognitive neuroscience research. With a stronger standing magnetic field, 7T MR scanners are capable of higher SNR than the more common 3 Tesla (3T) scanners, which can be used to push resolution higher for more anatomical specificity. Indeed, one of the previous functional connectivity investigations of the subcortical auditory system was conducted at 7T.

Within the field of functional connectivity analysis, moving beyond the traditional full correlation analysis should enable greater specificity in assessing functional connectivity patterns (Marrelec *et al.*, 2006; Smith, 2012). In particular, by identifying unique shared covariance between specific nodes in a network (and not other nodes in the network), partial correlation methods hold great promise for estimating direct functional connectivity within a network—in comparison to full correlations, which represent both direct and indirect connections (Smith, Beckmann, *et al.*, 2013). However, we are unaware of the application of such methods to assess functional connectivity within subcortical networks, particularly within the human auditory system.

In this article, we build on the prior Bayesian precision factor (PF) analysis model in Chandra et al. (2021) and develop a novel and highly robust Gaussian copula graphical model (GCGM) to assess functional connectivity. Using matrix-factorization based dimension-reduction techniques, the existing PF model can handle very high-dimensional problems far beyond the current state-of-the-art Bayesian methods in the literature of graphical models. However, it has the crucial assumption that each of the variables are marginally Gaussian distributed. Several studies in the literature have this assumption (Yu *et al.*, 2022; Zhang *et al.*, 2014). The Gaussian assumption has the useful implication that a zero partial correlation between two variables also means independence between them after removing the effects of other variables. However, in many applications—including ours—data are often not Gaussian distributed. The GCGM extends the PF model to the case where the univariate marginals can come from different distribution families. The association between the variables are modeled using a Gaussian copula that also implies conditional independence for zero partial correlation allowing easy interpretability of the conditional dependence graph.

Here, we use our novel GCGM approach to investigate functional connectivity between specific nodes across the human auditory system. We used publicly available 7T resting state fMRI from over one hundred participants to examine auditory connectivity. To probe connectivity within the auditory system, we included auditory cortical regions of interest as well as subcortical auditory regions derived from human histology (Sitek *et al.*, 2019). As the auditory pathway comprises a chain of multiple subcortical structures, and due to the largely lateralized organization of the auditory system, we hypothesized that partial correlations would be greatest between adjacent nodes in the same hemisphere, over and above the contributions from other auditory (and non-auditory) regions of interest. In particular, because of the critical position of auditory midbrain and thalamus as nexuses of bottom-up and top-down information transfer (Mihai *et al.*, 2019; Tabas *et al.*, 2021), we hypothesized strong partial correlations between inferior colliculus and medial geniculate. Overall, our findings demonstrate the methodological reliability of our GCGM approach as well as the neurobiological organization of auditory structures in the human auditory system.

2. Materials and methods

2.1 Magnetic resonance imaging acquisition and processing

We downloaded resting state fMRI from 106 participants in the 7T Human Connectome Project (Elam *et al.*, 2021; Van Essen *et al.*, 2012). Specifically, we utilized the minimally preprocessed volumetric data in common space (Glasser *et al.*, 2013). BOLD fMRI data were acquired with 1.6 mm isotropic voxel size across four runs of a resting state paradigm (repetition time [TR] = 1 s, 900 TRs per run). Two runs were acquired with anterior–posterior (AP) phase encoding, and two were acquired with posterior–anterior (PA) phase encoding.

For each individual and each run, we extracted mean timeseries from predefined regions of interest (ROIs). Subcortical auditory ROIs were defined using the Sitek–Gulban atlas (Sitek *et al.*, 2019). Cortical ROIs were defined using FreeSurfer's implementation of the DKT atlas (Dale *et al.*, 1999; Klein and Tourville, 2012). For this study we used transverse temporal gyrus (TTG) and superior temporal gyrus (STG) as auditory ROIs, as well as pericalcarine cortex (Calc) and superior frontal gyrus (SFG) as non-auditory control ROIs. Mean timeseries were extracted for each ROI using nilearn's [Masker] function. Subject and run-specific timeseries were then concatenated across subjects for each run (1–4).

2.2 Removing scanner drift

Strong temporal trends were observed in each ROI, a low-frequency artifact caused by minor instability of the fMRI scanner commonly known as scanner drift (Bianciardi *et al.*, 2009). Let $\mathrm{Y}_{\mathrm{i,j}}^{(\mathrm{t})}$ be the fMRI timeseries corresponding to the i-th individual's j-th ROI at the t-th timepoint. We average over the timeseries across the subjects (i.e. average the $\mathrm{Y}_{\mathrm{i,j}}^{(\mathrm{t})}$ over i) and plot the mean timeseries separately for each ROI and runs in Figure 1. A strong decreasing trend can be observed uniformly across all scenarios.

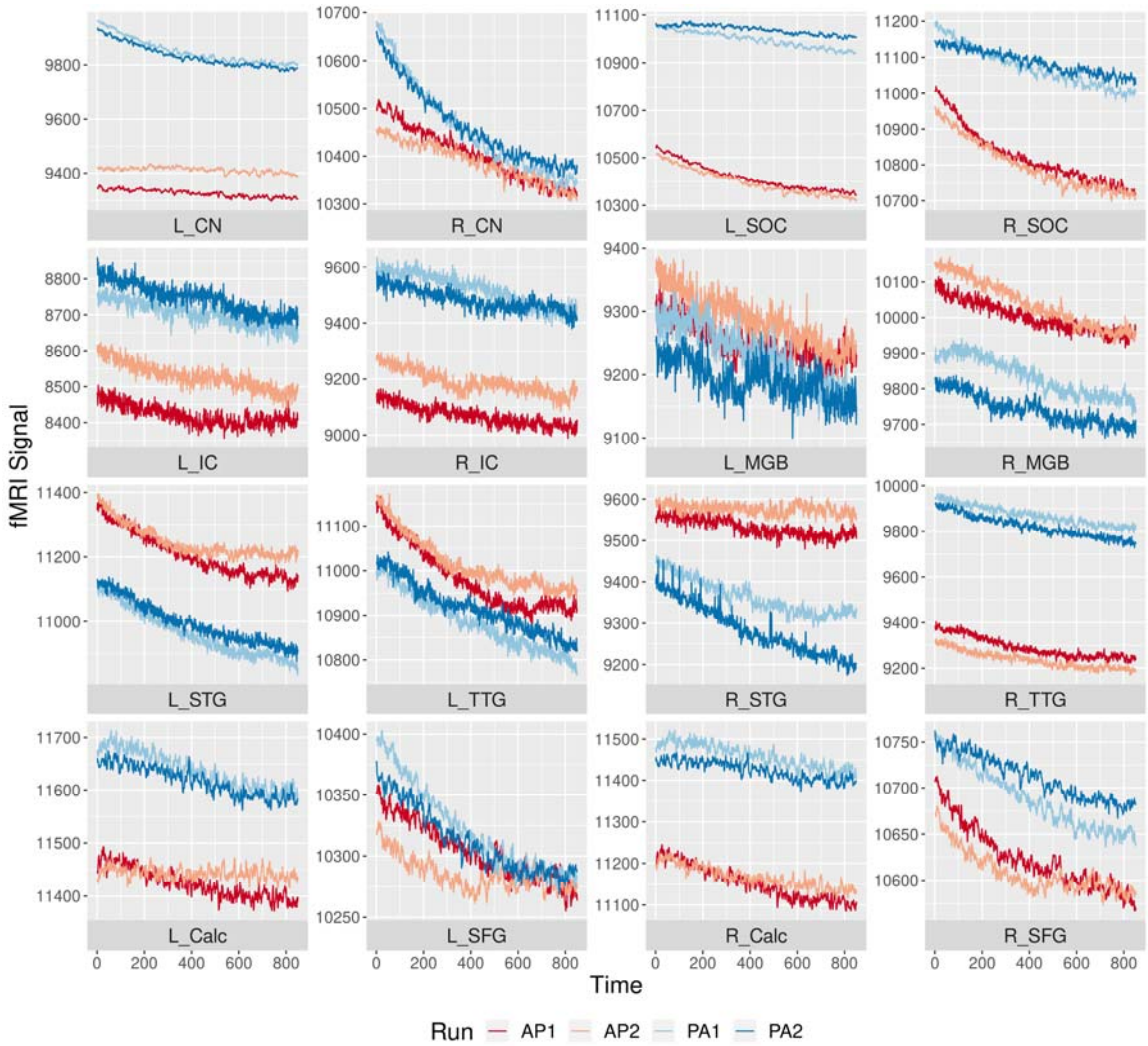

Figure 1 Scanner drift in different acquisition schemes: A strong decreasing trend can be observed when the timeserieses are averaged across the subjects for each acquisition scheme.

To remove this artifactual effect, we fit linear trend models on each of the mean timeseries separately for different ROIs and runs. Then we subtract the estimated linear trend from each individual's timeseries. In Figure 2 we illustrate the trend-removal pipeline with an example. We see that the decreasing trend induced by the scanner drift almost disappears from the individual timeseries after the trend-removal step.

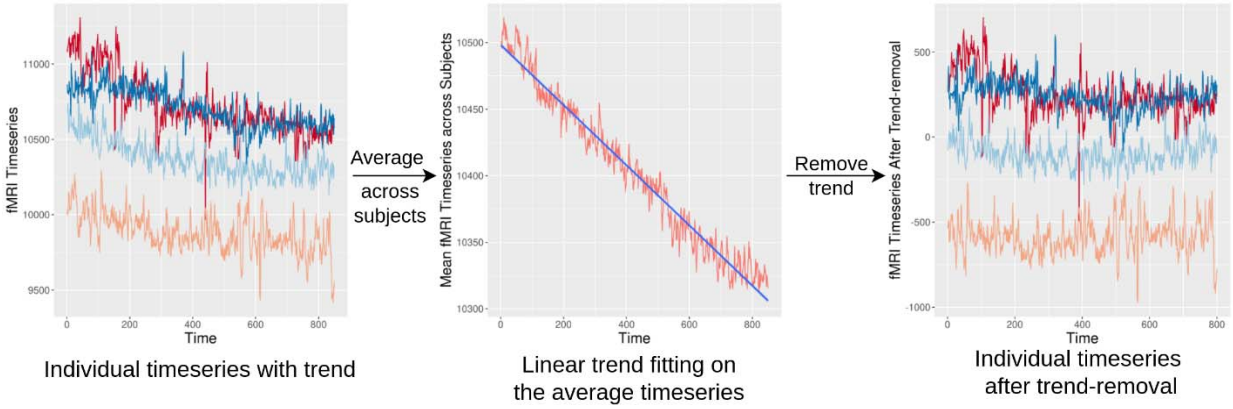

Figure 2 Linear trend removal pipeline: On the leftmost panel, timeserieses of some selected individuals have been plotted where a decresing trend can be observed uniformly across the subjects. On the middle panel, we plot the mean timeseries and fit a linear trend model to it. We subtract the fitted linear trend from the original timeserieses and again plot those in the rightmost panel. We can see that after the trend-removal procedure, the decresing trend almost disappears from the individual timeserieses.

2.3 Data partitioning and cross-validation

BOLD fMRI is prone to geometric distortions in the phase-encoding direction which can be largely corrected using a variety of methods (Esteban *et al.*, 2021; Jezzard and Balaban, 1995). Adjacent to motion-sensitive cerebrospinal fluid (CSF), the brainstem is particularly susceptible to such geometric distortions. Although the HCP minimal preprocessing pipeline corrects for phase-encoding distortions (Glasser *et al.*, 2013), to isolate the potential residual contribution of phase encoding direction on functional connectivity estimates, we conducted separate analyses on data collected with an anterior–posterior (AP) phase encoding direction (runs 1 and 3) and posterior–anterior (PA) phase encoding direction (runs 2 and 4). As opposed to (Smith, Vidaurre, *et al.*, 2013), we merge the fMRI timeseries from the subjects for each phase-encoding direction and performed partial correlation analysis on the merged dataset. We find this approach to reveal connectivity between auditory regions that could not have been identified in individual-specific analyzes.

We further interrogated our results using a leave-10%-out cross-validation (CV) approach. We assessed the stability of the connectivity estimates by checking the correlation between the results obtained from each acquisition scheme. *2.4 Gaussian copula graphical models*

The precision factor model, developed recently in (Chandra *et al.*, 2021), provided a novel computationally efficient robust technique for estimating sparse precision matrices. Since partial correlations can be readily obtained from the precision matrix, the approach allowed straightforward estimation of the underlying connectivity graphs. Their model however assumed the joint distribution of the data to be a zero mean multivariate Gaussian which implied that the univariate marginal distributions were also all Gaussians. The trend-removal makes the data mean centered but their marginal distributions still substantially deviate from the Gaussian distribution assumption of Chandra et al. (2021). In this paper, we therefore extend their model to accommodate non-Gaussian marginals as well.

Suppose we have d ROIs and Y_j be the observation corresponding to the j-th ROI with (unknown) marginal distribution f_j and corresponding cumulative distribution function (CDF) F_j. Copulas provide a broadly applicable class of tools that allow the joint distribution of $Y_1, \dots, Y_d$ to be flexibly characterized by first modeling the univariate marginals f_j's and then separately modeling their joint dependencies by mapping the $F_1(Y_1), \dots, F_d(Y_d)$ to a joint probability space. For Gaussian copulas, this is done by setting $Z_j = \Phi^{-1}\{F_j(Y_j)\}$, where $\Phi(\cdot)$ is the CDF of a standard Gaussian distribution. This implies marginally $Z_j \sim \mathrm{N}(0,1)$ for all $j = 1, \dots, d$, where $\mathrm{N}(\mu, \sigma^2)$ denotes a univariate Gaussian distribution with mean μ and variance σ^2. For their joint, we further assume

$$(Z_1, \dots, Z_d) \sim \mathrm{N}_d(0, R),$$

where R is a $d \times d$ order <u>correlation matrix</u>. Let $\Omega = \left(\left(\omega_{j,j'}\right)\right)$ be the corresponding precision matrix of $Z_1, \dots, Z_d$, that is, $R = \Psi^{-1/2}\Omega^{-1}\Psi^{-1/2}$ with $\Psi = \mathrm{diag}(\Omega^{-1})$. Then, by properties of copula and the simple multivariate Gaussian distribution, it can be shown that, irrespective of the form of the marginal f_j's, the ROIs Y_j and $Y_{j'}$ will be conditionally dependent on (and hence functionally connected with) each other given the rest if and only if $\omega_{j,j'} \neq 0$. This way, the precision matrix Ω characterizes the functional connectivities between the different Y_j's.

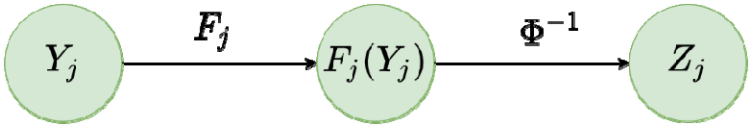

Figure 3 Copula model.

We model the unknown univariate marginal distributions of the 's using location-scale mixtures of Gaussians. Such mixtures can flexibly estimate a very large class of unknown densities (Ghosal *et al.*, 1999). Specifically, we let

(1)

where is the weight attached to the mixture component where with being a suitably chosen, moderately large, fixed integer.

To estimate the precision matrix , we consider the framework of Chandra et al. (2021). Recall that with . We next assume to admit a lower-rank plus diagonal (LRD) decomposition where is a order matrix and a diagonal matrix with positive 's. All positive definite matrices admit such a representation, in practice often sufficing to produce excellent approximations.

We take a Bayesian route to estimation and inference where we assign priors on the parameters of the proposed model and inference is based on samples drawn from the posterior using a Markov chain Monte Carlo (MCMC) algorithm. As was shown in Chandra et al. (2021), the LRD representation makes the MCMC very straightforward via a latent variable augmentation scheme.

2.5 Priors on the parameters

For the parameters of the mixture models specifying the marginals in equation (1), we consider the following priors

— —

where $(\mu, \sigma^2) \sim \mathrm{NIG}(\mu_0, \nu_0, a_0, b_0)$, implying that $\mu|\sigma^2 \sim \mathrm{N}(\mu_0, \nu_0^{-1}\sigma^2)$ and $\sigma^{-2} \sim \mathrm{Ga}(a_0, b_0)$, and $\mathrm{Ga}(a_0, b_0)$ is a gamma distribution with mean a_0/b_0 and variance a_0/b_0^2.

We assign a two-parameter generalization of the Dirichlet-Laplace (DL) prior from Bhattacharya et al. (Bhattacharya *et al.*, 2015) that allows more flexible tail behavior on the elements of Λ. On a d-dimensional vector θ, our DL prior with parameters a and b, denoted by $\mathrm{DL}(a, b)$, can be specified in the following hierarchical manner

$$\theta_j \mid \psi, \phi, \tau \overset{ind}{\sim} \mathrm{N}\left(0, \psi_j \phi_j^2 \tau^2\right), \psi_j \overset{iid}{\sim} \mathrm{Exp}(1/2), \phi \sim \mathrm{Dir}(a, \ldots, a), \tau \sim \mathrm{Ga}(da, b),$$

where θ_j is the j-th element of θ, ϕ and ψ are vectors of same length as θ, $\mathrm{Exp}(a)$ is an exponential distribution with mean $1/a$, $\mathrm{Dir}(a_1, \ldots, a_d)$ is a d-dimensional Dirichlet distribution. The original DL prior is a special case with $b = 1/2$. We let $\mathrm{vec}(\Lambda) \sim \mathrm{DL}(a, b)$.

The d distinct δ_j^2 's may result in over-parametrization. To reduce the effective number of parameters in an adaptive manner, we use a Dirichlet process (DP) prior (Ferguson, 1973) on the δ_j^2's as $\delta_j^2|G \overset{iid}{\sim} G, G|\alpha \sim \mathrm{DP}(\alpha, G_0)$ with $G_0 = \mathrm{Ga}(a_\delta, b_\delta), \alpha \sim \mathrm{Ga}(a_\alpha, b_\alpha)$,where α is the concentration parameter and G_0 is the base measure. The DP model allows clustering the δ_j^2's allowing for additional data-adaptive parameter reduction. We discussed a Markov chain monte Carlo (MCMC) based implementation strategy of our model in the supplementary materials.

3. Results

3.1 Partial correlations between regions of interest

Using our copula graphical model approach, we first estimated the precision matrix Ω and subsequently computed the partial correlations. We reported the significant edges subject to controlling the posterior false discovery rate (Sarkar *et al.*, 2008) at the 10% level. We found that the strongest auditory connectivity was between adjacent structures in the same hemisphere, particularly between the auditory midbrain (inferior colliculus, or IC) and thalamus (medial geniculate body, or MGB) and between core and associative auditory cortex (TTG and STG). We also saw strong connectivity between homologous control regions (i.e., between left

and right calcarine cortex, and between left and right SFG). Weaker (but still present) connectivity was observed between homologous auditory structures, particularly in midbrain and thalamus. Weak connectivity was present between adjacent brainstem auditory structures (cochlear nucleus [CN] and superior olivary complex [SOC]) on the left (but not right). Interestingly, despite the SOC being the primary (and earliest) decussation point in the ascending auditory pathway, we did not observe partial correlations between contralateral CN and SOC.

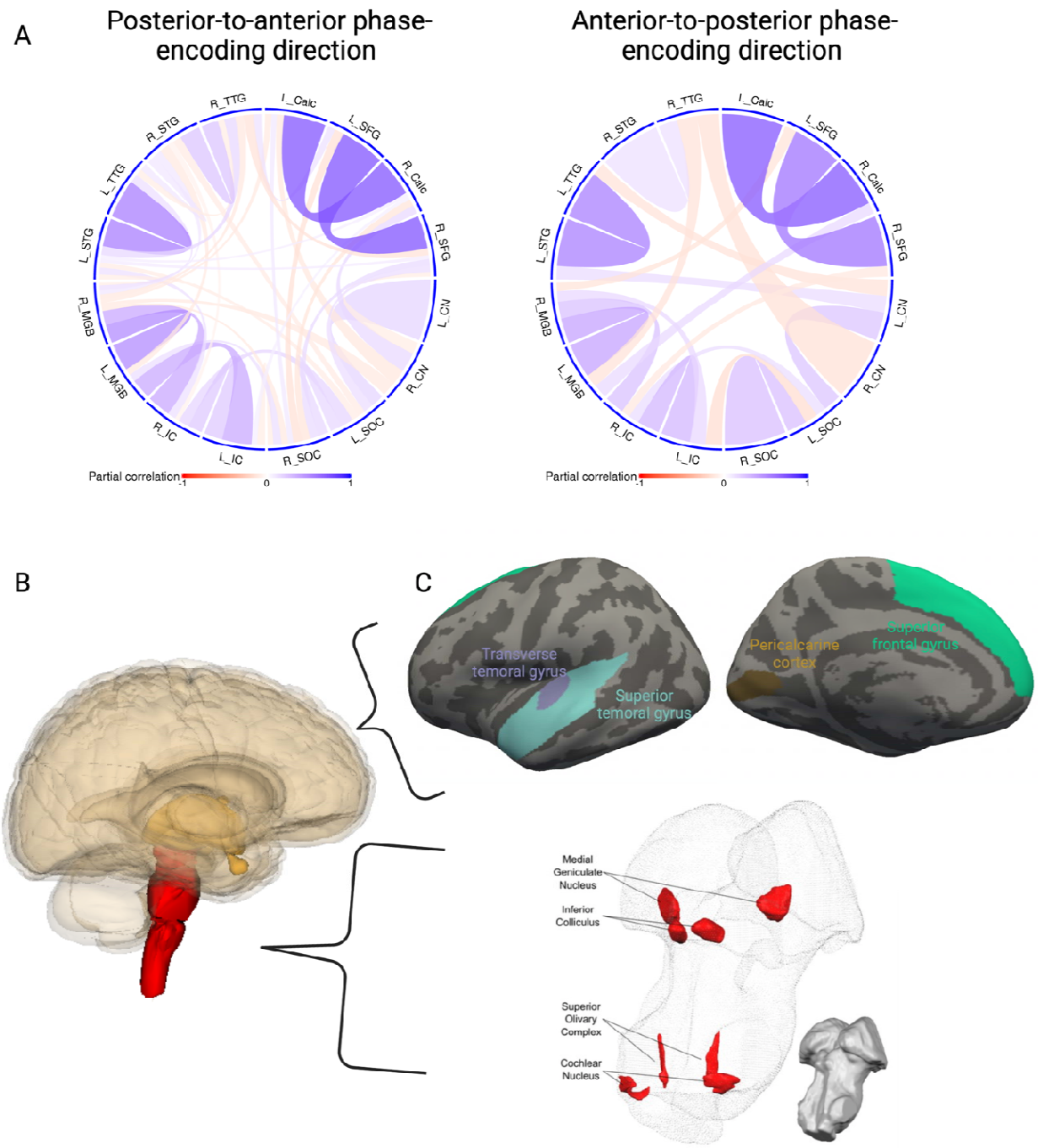

263

Figure 4. A: Partial correlation connectivity in data acquired with posterior-to-anterior (PA; left) and anterior-to-posterior (AP; right) phase-encoding directions. B: 3-dimensional view of the human brain with the brainstem highlighted in red. C: regions of interest from which functional timeseries were extracted. Top: cortical regions from FreeSurfer's DKT atlas. Bottom: subcortical auditory regions (Sitek et al., 2019).

3.2 Effect of phase encoding scheme on subcortical connectivity

Due to the anatomical location of the subcortical auditory structures—in dense, heterogeneous subcortical regions and largely adjacent to CSF—we conducted connectivity analyses separately on AP- and PA-acquired fMRI runs. We then compared the connectivity results from the two acquisition schemes. Overall connectivity patterns were highly similar between the two phase-encoding schemes (Figure 4; Pearson's $r = 0.805$, $p < 0.001$). Subcortical connectivity was quite robust between the brainstem auditory regions (except for left and right CN), as was cortical connectivity (with the exception of right TTG and right STG).

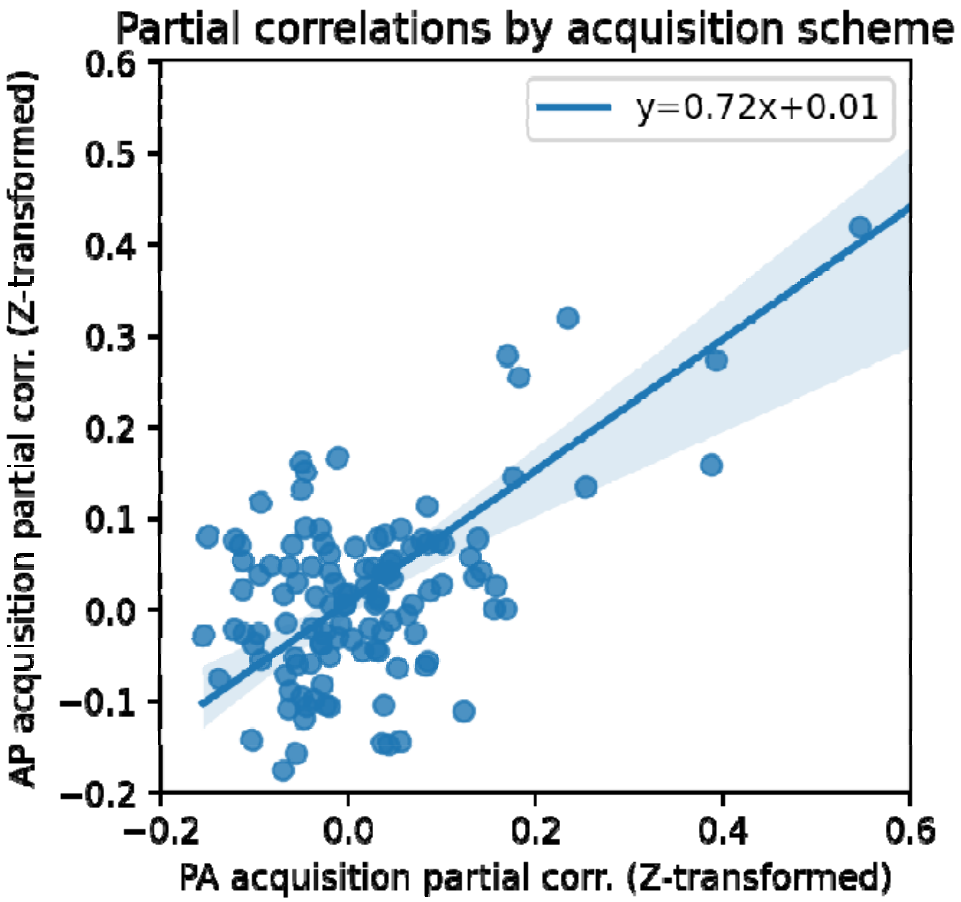

Figure 5. Pearson correlation of partial correlation values between posterior-to-anterior and anterior-to-posterior phase-encoding acquisition schemes across all edges in the graph (region-to-region connections).

3.3 Cross-validation of partial correlations

To assess the stability of our partial correlation results, we ran leave-10%-out cross-validation within each phase encoding scheme and computed (full) correlations across the 10 folds per scheme (for a total of 20 folds; see Figure 6). Across all folds (and both phase encoding schemes), the results were highly similar (intraclass correlation of edgewise partial correlations across cross-validation folds = 0.912).

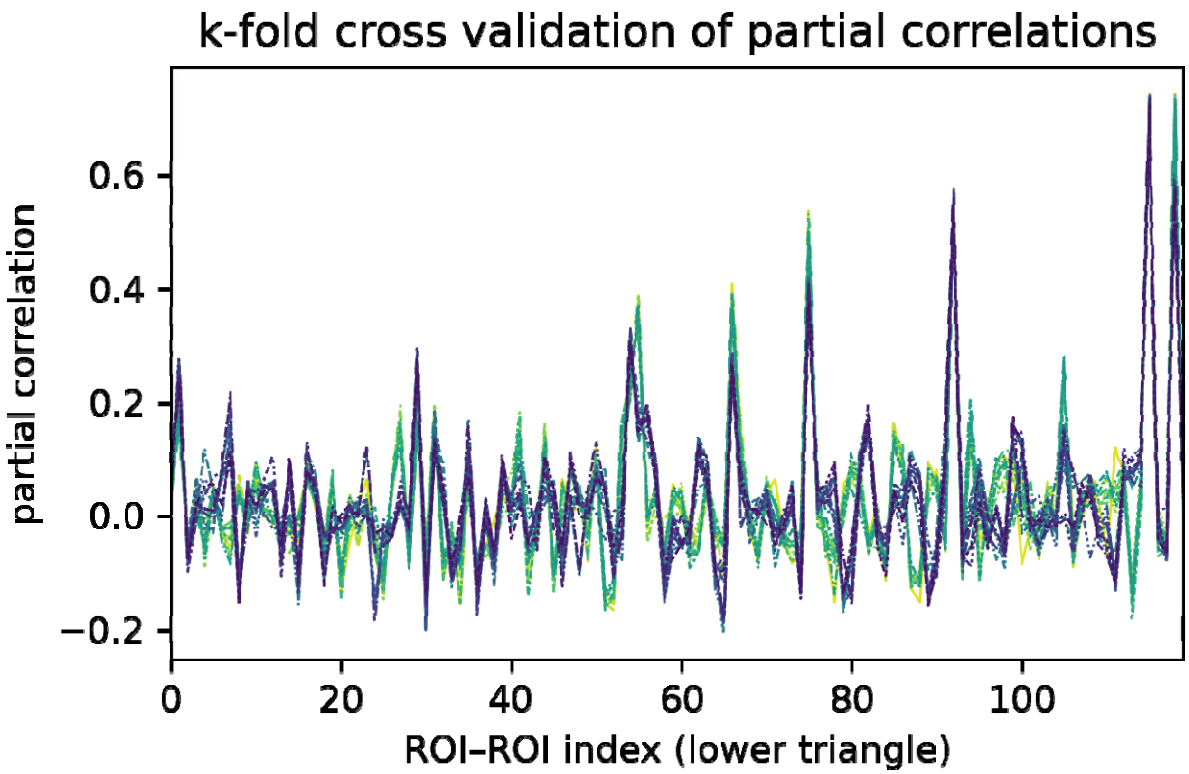

Figure 6. Partial correlations across cross-validation folds (10 folds for each of the two phase-encoding acquisition schemes).

3.4 Fit of the copula graphical model

We studied the goodness-of-fit of the copula graphical model. In Figure 7 we plotted the sample histogram and the corresponding fitted marginal densities for some selected ROIs. The sample histograms strongly indicated that distribution of the data substantially deviate from the Gaussian assumption. The following figure shows that our flexible location-scale mixture of Gaussians fit the data very well even though marginally the data are not Gaussian distributed.

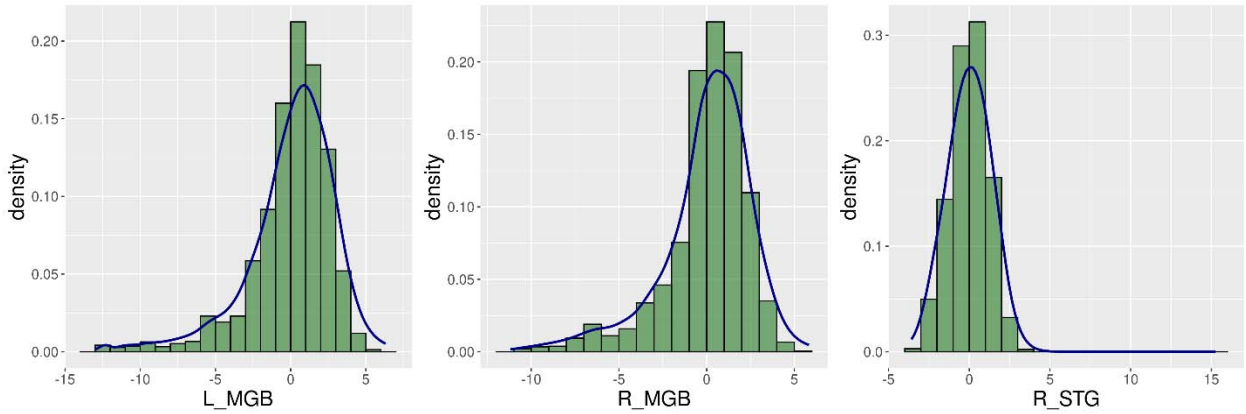

Figure 7 Marginal fits for the location-scale mixture of Gaussian distributions: The sample histograms in green clearly showed that distribution of the ROIs substantially deviates from Gaussian assumption. The blue lines are the respective fitted densities corresponding to the mixture model in eqn (1). These figures indicate excellent goodness-of-fit.

3.5 Comparison with existing approaches

We compared with two standard approaches in the literature: (1) analyzing the graphs for each subject separately and then combining them (Smith, Vidaurre, *et al.*, 2013); and (2) the precision factor model (Chandra *et al.*, 2021) that assumes Gaussian distribution on the BOLD signals corresponding to each ROI. In both comparisons, we did separate analyzes for each of the acquisition schemes.

For comparison (1) the results are provided in Figure 8. While the strongest edges in the network can be recovered, we can see that the weak edges are mostly absent compared to Figure 4 (for instance, between IC and MGB). Due to the low signal-to-noise ratio in fMRI timeseries in small, deep subcortical structures, the weak edges cannot be recovered from the individual-specific analyzes.

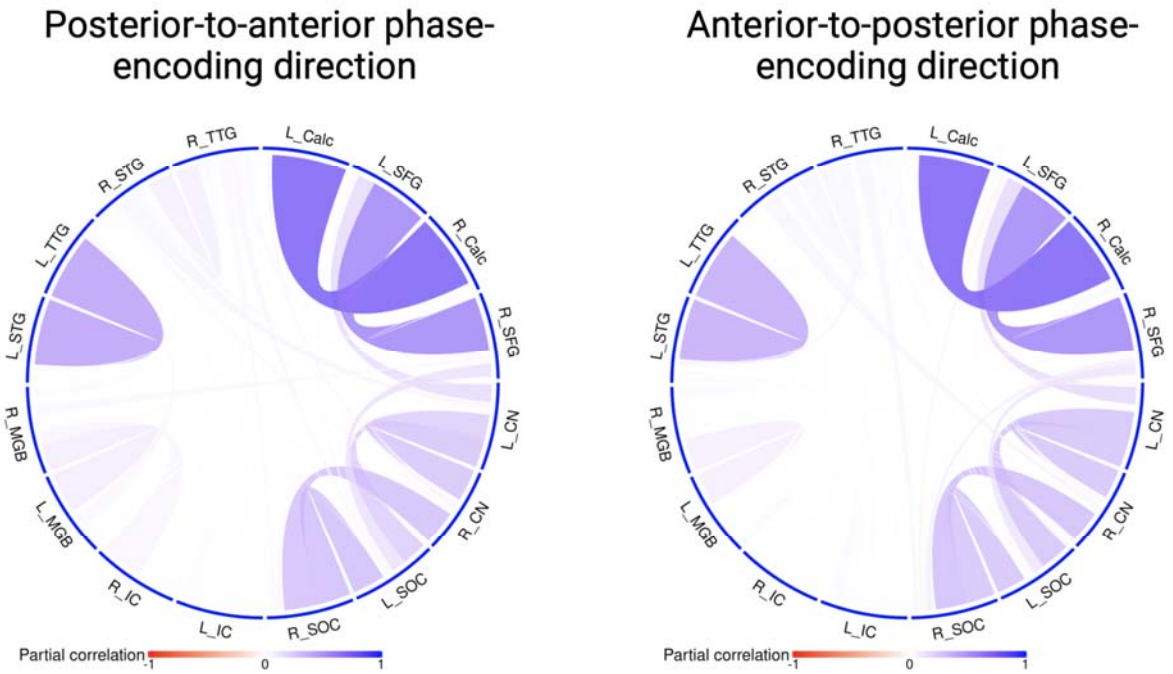

Figure 8 Conditional dependency graph for comparison (1): BOLD signals for each subject are analyzed separately and the average graphs are reported for each of the acquisition schemes.

Results corresponding to comparison (2) are provided in Figure 9. Graphs corresponding to the posterior-to-anterior phase encoding detection majorly differ between the Gaussian graphical model and the copula graphical model with the former being much denser. This is a common phenomenon for graphical models if the Gaussian assumption is made on non-Gaussian distributed data; see, e.g., Section 5, example 1(a) in (Guha *et al.*, 2020). In Figure 10 we plot the marginal Gaussian fits on the histograms of some BOLD signals. Clearly the simple Gaussian assumption does not hold here and more flexible model like the copula graphical model is required.

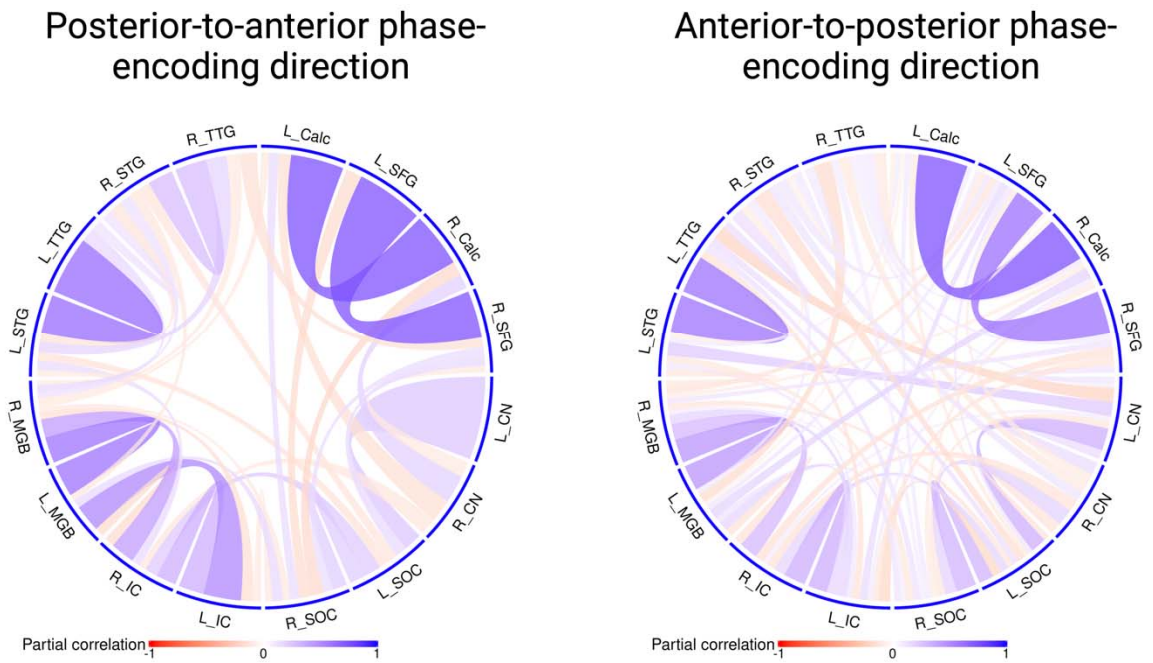

Figure 9 Conditional dependency graph for comparison (2): Instead of the proposed copula graphical model, the precision factor model in (Chandra *et al.*, 2021) *with Gaussian assumption on the marginal distribution of the BOLD signals corresponding to each ROI.*

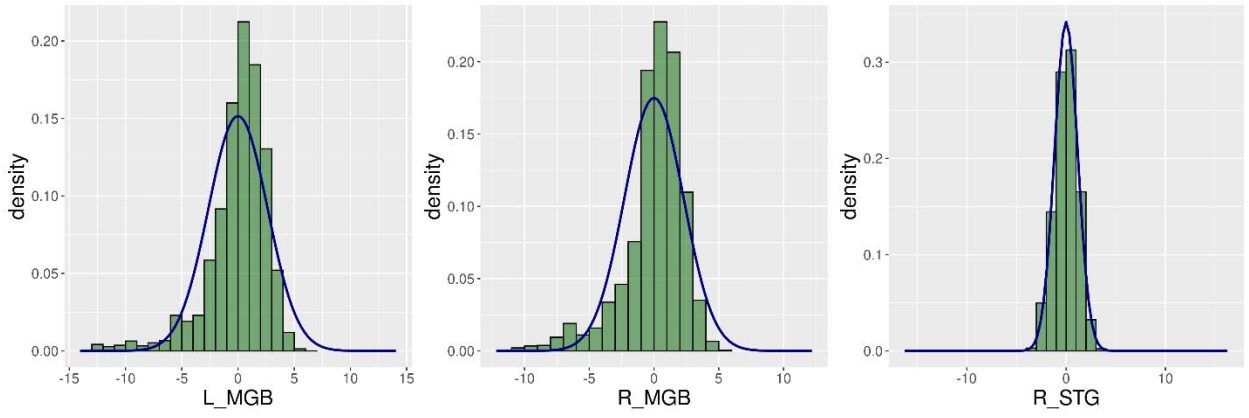

Figure 10 Marginal Gaussian fits (blue lines) on the BOLD signals (green histograms) for some selected ROIs. High skewness in the BOLD histograms suggests that the Gaussian assumption does not hold for these data.

4. Discussion

The mammalian auditory pathway consists of a chain of interconnected subcortical and cortical brain structures. Assessing the connectivity of the human subcortical auditory structures has been limited due to methodological challenges of non-invasive imaging of the deep, small structures. Recent acquisition and analytical advances enable finer grained investigations of connectivity throughout the brain, including the brainstem. In this work, we developed a novel approach to estimating partial correlations using copula graphical models to a publicly available high-resolution resting state functional MRI dataset. We found highly consistent connectivity patterns between auditory brain regions that demonstrates the efficacy of our connectivity method as well as the potential for functional connectivity investigations of the subcortical auditory system.

Using partial correlations (as opposed to full correlations) allows us to identify specific relationships between nodes in a connectivity graph by removing shared variance across nodes as illustrated in the stylized example in the supplementary materials.

To model and learn the dependence structure between the regions of interest in this analysis, we implemented a Gaussian copula graphical model, which can be used for non-Gaussian distributed data as well, such as functional MRI data. In this study, we found strong partial correlations in resting state functional MRI data between cochlear nucleus (CN) and superior olivary complex (SOC) in the left hemisphere (but not in the right). These connectivity patterns between CN and SOC have not been observed in human auditory brainstem but follow our understanding of the mammalian auditory pathway based on research in animal models. Principally, auditory information that is transduced by the cochlea of each ear is transmitted via the cochlear nerve to the cochlear nucleus, the first stage of the central auditory pathway, on each side of the brainstem. From there, auditory signals are passed to both the ipsilateral and contralateral SOC for further auditory processing, including spatial localization (Moore, 2000). Interestingly, we only observed left CN–SOC connectivity (and in both data acquisition schemes). It is unclear why similar patterns were not observed between right CN and SOC or between contralateral structures (left CN to right SOC and right CN to left SOC). One contributor is the lower signal-to-noise ratio in MRI data from the lower brainstem. Paired with

346 the small size of each of the brainstem auditory nuclei, we may still be at the edge of what is
347 detectable using present functional connectivity methods. Further, ipsilateral connections (e.g.,
348 between left CN and left SOC) may be stronger due to their close physical proximity. Even with
349 relatively high 1.05 mm spatial resolution 7T fMRI data, CN and SOC on each side are only
350 separated by a few voxels. These regions are thus at increased likelihood of sharing temporal
351 fluctuations due to partial volume effects, wide point-spread functions, non-Gaussian spatial
352 dependence, imperfect image registration, or other as-yet-unsolved fMRI confounds that are
353 particularly acute in the lower brainstem.

354 Moving up the primary auditory pathway, we found significant partial correlations between left
355 SOC and right inferior colliculus (IC) in each acquisition scheme. Due to crossing connections at
356 the level of the SOC, such contralateral connectivity is to be expected. The lack of right SOC to
357 left IC connectivity is odd, but when considered with the previous results—an absence of right
358 CN to right SOC connectivity—this suggests that right CN was particularly affected by low MRI
359 SNR in the brainstem. Further, both sets of data showed strong partial correlations between
360 left and right IC. Anatomically, IC contains a strong white matter bundle—the commissure of
361 IC—connecting left and right IC. Thus, the significant functional connectivity between the two
362 colliculi fits nicely with neuroanatomical features.

363 Passing information to the next level of the auditory pathway, we observed significant partial
364 correlations between left IC and left medial geniculate body (MGB) of the thalamus in the
365 posterior-to-anterior acquisition scheme and between right IC and right MGB in both phase-
366 encoding schemes. Interestingly, we found strong partial correlations between left and right
367 MGB in both datasets. Although not directly connected by large white matter bundles, left and
368 right MGB are expected to process auditory information from IC at similar levels of abstraction.
369 Thus, partial correlations may reflect indirect but shared neural mechanisms of auditory
370 processing in the thalamus.

371 Finally in auditory cortex, left transverse temporal gyrus (TTG)—the location of primary
372 auditory cortex—was strongly connected with left superior temporal gyrus (STG), which
373 contains secondary and associative auditory cortices. A homologous connectivity pattern was
374 found between right TTG and STG, but only in the posterior-to-anterior acquisition scheme.

These functional connectivity results align with a vast literature demonstrating information flow between primary and non-primary auditory cortex (for review, see (Hackett, 2011).

In non-auditory cortical regions (superior frontal gyrus and calcarine cortex), we observed strong partial correlations between contralateral homologues, as would be expected based on prior literature of bilateral symmetry of functional connectivity patterns. These contrahemispheric connections were missing from auditory cortex regions perhaps due to the inclusion of multiple auditory cortical regions, as the partial correlation approach removes variance that is shared across the network and leaves only the strongest region-to-region connectivity. Complementarily, some literature suggests that left and right auditory cortex process auditory information at distinct timescales and levels of abstraction (Güntürkün *et al.*, 2020; Hickok and Poeppel, 2007; Zatorre *et al.*, 2002), with left auditory cortex being uniquely tuned to rapidly changing temporal information—such as the phonetics of speech sounds—while right auditory cortex is more sensitive to slower changes in the spectral domain, particularly for speech prosody as well as music.

Overall, the present study is one of the first investigations into functional MRI connectivity across the entire human auditory system. To date, there have been only limited applications of functional MRI methods to study subcortical auditory connectivity (Berlot *et al.*, 2020; Hofmeier *et al.*, 2018). Due to the small size of the subcortical auditory structures, high spatial resolution is highly beneficial for anatomical segmentation of the structures. However, increasing the resolution of MRI scans results in decreased SNR in each voxel, requiring greater amounts of MRI data to achieve reasonable fMRI contrast. In this study, we took advantage of the large amounts of high-resolution data collected in the 7-Tesla Human Connectome Project (HCP; four runs of 900 BOLD volumes with TR = 1 s at 1.6 mm isotropic spatial resolution) in order to identify connectivity patterns between auditory structures.

As the HCP data were collected in two phase-encoding acquisition schemes, we were able to investigate the potential influence of phase-encoding direction on subcortical auditory connectivity. Due to the location of subcortical auditory structures along the dorsal brainstem and midbrain—near or adjacent to ventricles that are known to conduct physiological motion—it was unknown whether correction for susceptibility distortion (as part of the HCP minimal

preprocessing pipeline) was sufficient. In the present study, we found minimal differences between the two acquisition schemes after susceptibility distortion correction, reinforcing the efficacy of such methods for investigating subcortical (particularly brainstem) connectivity.

5. Conclusions

Using a Gaussian copula-based novel approach to partial correlation estimation, we identified functional connectivity in the human auditory system using resting state functional MRI. In particular, brainstem connectivity was highly consistent across acquisitions, demonstrating the utility and applicability of functional connectivity methods in deep brain structures. Future research will investigate global partial correlation connectivity using this Gaussian graphical model approach.

References

Bibliography

Abrams DA, Kochalka J, Bhide S, Ryali S, Menon V. Intrinsic functional architecture of the human speech processing network. Cortex 2020; 129: 41–56.

Berlot E, Arts R, Smit J, George E, Gulban OF, Moerel M, et al. A 7 Tesla fMRI investigation of human tinnitus percept in cortical and subcortical auditory areas. Neuroimage Clin. 2020; 25: 102166.

Bhattacharya A, Pati D, Pillai NS, Dunson DB. Dirichlet-Laplace priors for optimal shrinkage. J. Am. Stat. Assoc. 2015; 110: 1479–1490.

Bianciardi M, Fukunaga M, van Gelderen P, Horovitz SG, de Zwart JA, Shmueli K, et al. Sources of functional magnetic resonance imaging signal fluctuations in the human brain at rest: a 7 T study. Magn. Reson. Imaging 2009; 27: 1019–1029.

Biswal B, Yetkin FZ, Haughton VM, Hyde JS. Functional connectivity in the motor cortex of resting human brain using echo-planar MRI. Magn. Reson. Med. 1995; 34: 537–541.

Cha K, Zatorre RJ, Schönwiesner M. Frequency Selectivity of Voxel-by-Voxel Functional Connectivity in Human Auditory Cortex. Cereb. Cortex 2016; 26: 211–224.

Chandra NK, Mueller P, Sarkar A. Bayesian Scalable Precision Factor Analysis for Massive Sparse Gaussian Graphical Models. arXiv 2021: arXiv:2107.11316.

Chechik G, Nelken I. Auditory abstraction from spectro-temporal features to coding auditory entities. Proc. Natl. Acad. Sci. USA 2012; 109: 18968–18973.

436 Chen J, Hu B, Qin P, Gao W, Liu C, Zi D, et al. Altered brain activity and functional connectivity in
437 unilateral sudden sensorineural hearing loss. Neural Plast. 2020; 2020: 9460364.

438 Dale AM, Fischl B, Sereno MI. Cortical surface-based analysis. I. Segmentation and surface
439 reconstruction. Neuroimage 1999; 9: 179–194.

440 De Martino F, Moerel M, van de Moortele P-F, Ugurbil K, Goebel R, Yacoub E, et al. Spatial
441 organization of frequency preference and selectivity in the human inferior colliculus. Nat.
442 Commun. 2013; 4: 1386.

443 Eckert MA, Kamdar NV, Chang CE, Beckmann CF, Greicius MD, Menon V. A cross-modal system
444 linking primary auditory and visual cortices: evidence from intrinsic fMRI connectivity analysis.
445 Hum. Brain Mapp. 2008; 29: 848–857.

446 Elam JS, Glasser MF, Harms MP, Sotiropoulos SN, Andersson JLR, Burgess GC, et al. The Human
447 Connectome Project: A retrospective. Neuroimage 2021; 244: 118543.

448 Esteban O, Adebimpe A, Markiewicz CJ, Goncalves M, Blair RW, Cieslak M, et al. The Bermuda
449 Triangle of d- and f-MRI sailors - software for susceptibility distortions (SDCFlows). 2021

450 Ferguson TS. A Bayesian Analysis of Some Nonparametric Problems on JSTOR [Internet].
451 1973[cited 2022 May 10] Available from: https://www.jstor.org/stable/2958008

452 Ghosal S, Ghosh JK, Ramamoorthi RV. Posterior consistency of Dirichlet mixtures in density
453 estimation. Ann. Statist. 1999; 27

454 Glasser MF, Sotiropoulos SN, Wilson JA, Coalson TS, Fischl B, Andersson JL, et al. The minimal
455 preprocessing pipelines for the Human Connectome Project. Neuroimage 2013; 80: 105–124.

456 Gordon EM, Laumann TO, Adeyemo B, Petersen SE. Individual Variability of the System-Level
457 Organization of the Human Brain. Cereb. Cortex 2017; 27: 386–399.

458 Guha N, Baladandayuthapani V, Mallick BK. Quantile Graphical Models: a Bayesian Approach.
459 Journal of Machine Learning Research 2020

460 Güntürkün O, Ströckens F, Ocklenburg S. Brain lateralization: A comparative perspective.
461 Physiol. Rev. 2020; 100: 1019–1063.

462 Hackett TA. Information flow in the auditory cortical network. Hear. Res. 2011; 271: 133–146.

463 Hawley ML, Melcher JR, Fullerton BC. Effects of sound bandwidth on fMRI activation in human
464 auditory brainstem nuclei. Hear. Res. 2005; 204: 101–110.

465 Hickok G, Poeppel D. The cortical organization of speech processing. Nat. Rev. Neurosci. 2007;
466 8: 393–402.

467 Hofmeier B, Wolpert S, Aldamer ES, Walter M, Thiericke J, Braun C, et al. Reduced sound-
468 evoked and resting-state BOLD fMRI connectivity in tinnitus. Neuroimage Clin. 2018; 20: 637–
469 649.

470 Jezzard P, Balaban RS. Correction for geometric distortion in echo planar images from B0 field
471 variations. Magn. Reson. Med. 1995; 34: 65–73.

472 Klein A, Tourville J. 101 labeled brain images and a consistent human cortical labeling protocol.

473 Front. Neurosci. 2012; 6: 171.

474 Leaver AM, Turesky TK, Seydell-Greenwald A, Morgan S, Kim HJ, Rauschecker JP. Intrinsic
475 network activity in tinnitus investigated using functional MRI. Hum. Brain Mapp. 2016; 37:
476 2717–2735.

477 Marrelec G, Krainik A, Duffau H, Pélégrini-Issac M, Lehéricy S, Doyon J, et al. Partial correlation
478 for functional brain interactivity investigation in functional MRI. Neuroimage 2006; 32: 228–
479 237.

480 Maudoux A, Lefebvre P, Cabay J-E, Demertzi A, Vanhaudenhuyse A, Laureys S, et al. Auditory
481 resting-state network connectivity in tinnitus: a functional MRI study. PLoS One 2012; 7:
482 e36222.

483 Mihai PG, Moerel M, de Martino F, Trampel R, Kiebel S, von Kriegstein K. Modulation of
484 tonotopic ventral medial geniculate body is behaviorally relevant for speech recognition. Elife
485 2019; 8

486 Miletić S, Bazin PL, Weiskopf N, Van der Zwaag W, Forstmann BU, Trampel R. fMRI protocol
487 optimization for simultaneously studying small subcortical and cortical areas at 7 T. Neuroimage
488 2020: 116992.

489 Moerel M, De Martino F, Uğurbil K, Yacoub E, Formisano E. Processing of frequency and
490 location in human subcortical auditory structures. Sci. Rep. 2015; 5: 17048.

491 Moore JK. Organization of the human superior olivary complex. Microsc. Res. Tech. 2000

492 Power JD, Cohen AL, Nelson SM, Wig GS, Barnes KA, Church JA, et al. Functional network
493 organization of the human brain. Neuron 2011; 72: 665–678.

494 Preibisch C, Castrillón G JG, Bührer M, Riedl V. Evaluation of Multiband EPI Acquisitions for
495 Resting State fMRI. PLoS One 2015; 10: e0136961.

496 Ren J, Xu T, Wang D, Li M, Lin Y, Schoeppe F, et al. Individual variability in functional
497 organization of the human and monkey auditory cortex. Cereb. Cortex 2021; 31: 2450–2465.

498 Ress D, Chandrasekaran B. Tonotopic organization in the depth of human inferior colliculus.
499 Front. Hum. Neurosci. 2013; 7: 586.

500 Sarkar SK, Zhou T, Ghosh D. A General Decision Theoretic Formulation of Procedures Controlling
501 FDR and FNR from a Bayesian Perspective. Stat Sin 2008; 18

502 Sigalovsky IS, Melcher JR. Effects of sound level on fMRI activation in human brainstem,
503 thalamic and cortical centers. Hear. Res. 2006; 215: 67–76.

504 Sitek KR, Gulban OF, Calabrese E, Johnson GA, Lage-Castellanos A, Moerel M, et al. Mapping the
505 human subcortical auditory system using histology, postmortem MRI and in vivo MRI at 7T. Elife
506 2019; 8

507 Smith SM. The future of FMRI connectivity. Neuroimage 2012; 62: 1257–1266.

508 Smith SM, Beckmann CF, Andersson J, Auerbach EJ, Bijsterbosch J, Douaud G, et al. Resting-
509 state fMRI in the Human Connectome Project. Neuroimage 2013; 80: 144–168.

Smith SM, Vidaurre D, Beckmann CF, Glasser MF, Jenkinson M, Miller KL, et al. Functional connectomics from resting-state fMRI. Trends Cogn. Sci. (Regul. Ed.) 2013; 17: 666–682.

Tabas A, Kiebel S, Marxen M, von Kriegstein K. Fast frequency modulation is encoded according to the listener expectations in the human subcortical auditory pathway. arXiv 2021

Van Essen DC, Ugurbil K, Auerbach E, Barch D, Behrens TEJ, Bucholz R, et al. The Human Connectome Project: a data acquisition perspective. Neuroimage 2012; 62: 2222–2231.

Yu Z, Guindani M, Grieco SF, Chen L, Holmes TC, Xu X. Beyond t test and ANOVA: applications of mixed-effects models for more rigorous statistical analysis in neuroscience research. Neuron 2022; 110: 21–35.

Zatorre R, Belin P, Penhune VB. Structure and function of auditory cortex: music and speech. Trends Cogn. Sci. (Regul. Ed.) 2002; 6: 37–46.

Zhang J, Chen Y-C, Feng X, Yang M, Liu B, Qian C, et al. Impairments of thalamic resting-state functional connectivity in patients with chronic tinnitus. Eur. J. Radiol. 2015; 84: 1277–1284.

Zhang L, Guindani M, Versace F, Vannucci M. A spatio-temporal nonparametric Bayesian variable selection model of fMRI data for clustering correlated time courses. Neuroimage 2014; 95: 162–175.